

# Magnetotransport properties of the type II Weyl semimetal candidate $\text{Ta}_3\text{S}_2$

D. Chen<sup>1,2</sup>, L. X. Zhao<sup>2</sup>, J. B. He<sup>2</sup>, H. Liang<sup>2</sup>, S. Zhang<sup>2</sup>, C. H. Li<sup>2</sup>, L. Shan<sup>2,3</sup>, S. C. Wang<sup>1</sup>, Z. A. Ren<sup>2,3</sup>, C. Ren<sup>2,5</sup>, and G. F. Chen<sup>2,3,4†</sup>

<sup>1</sup>*Department of Physics, Renmin University of China, Beijing 100872, China*

<sup>2</sup>*Institute of Physics and Beijing National Laboratory for Condensed Matter Physics, Chinese Academy of Sciences, Beijing 100190, China*

<sup>3</sup>*Collaborative Innovation Center of Quantum Matter, Beijing, China*

<sup>4</sup>*School of Physical Sciences, University of Chinese Academy of Sciences, Beijing 100190, China and*

<sup>5</sup>*Physics Department, Yunnan University, Kunming 671000, China*

We have investigated the magnetoresistance (MR) and Hall resistivity properties of the single crystals of tantalum sulfide,  $\text{Ta}_3\text{S}_2$ , which was recently predicted to be a new type II Weyl semimetal. Large MR (up to  $\sim 8000\%$  at 2 K and 16 T), field-induced metal-insulator-like transition and nonlinear Hall resistivity are observed at low temperatures. The large MR shows a strong dependence on the field orientation, leading to a giant anisotropic magnetoresistance (AMR) effect. For the field applied along the  $b$ -axis ( $B \parallel b$ ), MR exhibits quadratic field dependence at low fields and tends towards saturation at high fields; while for  $B \parallel a$ , MR presents quadratic field dependence at low fields and becomes linear at high fields without any trend towards saturation. The analysis of the Hall resistivity data indicates the coexistence of a large number of electrons with low mobility and a small number of holes with high mobility. Shubnikov-de Haas (SdH) oscillation analysis reveals three fundamental frequencies originated from the three-dimensional (3D) Fermi surface (FS) pockets. We find that the semi-classical multiband model is sufficient to account for the experimentally observed MR in  $\text{Ta}_3\text{S}_2$ .

## INTRODUCTION

The recent discovery of Weyl and Dirac semimetals (WSM/DSM) has attracted much attention in condensed matter physics and material science [1–11]. These materials, having a linear dispersion at the crossing of the valence and conduction bands near the Fermi energy, can be considered as three-dimensional (3D) analogues of graphene [12]. By breaking either time-reversal symmetry or inversion symmetry, DSM can also evolve to WSM and the Weyl nodes with specific chirality can be viewed as the magnetic monopole in momentum space [13]. The WSM has been classified into two types [7, 14]. The type I WSM exhibits ideal conical Weyl cone with Lorentz symmetry. While in type II WSM, the Weyl cone is extreme tilted and Lorentz symmetry is violated. Experimentally, Fermi arc has been detected by the angle resolved photoemission spectroscopy (ARPES) measurements for both two types of materials [9, 10, 15, 16], while the negative longitudinal magnetoresistance (MR) has been observed only for the type I WSM [8, 17, 18]. Although some exotic properties like novel anomalous Hall effect (AHE) has been theoretically predicted for the type II WSM [19], it is not experimentally verified yet. It remains an important challenge to find more new materials and to study the unusual magnetotransport properties and the unique electronic structure.

Tantalum sulfide  $\text{Ta}_3\text{S}_2$  was predicted to be a robust type II WSM candidate with 8 Weyl nodes [20]. The  $k$ -space separation between Weyl nodes of  $\text{Ta}_3\text{S}_2$  is the largest among the known Weyl semimetal candidates. As shown in Fig. 1(a),  $\text{Ta}_3\text{S}_2$  crystalizes in an orthorhombic

structure without inversion symmetry, which is the key to realizing the Weyl semimetal state. Transport properties of polycrystalline  $\text{Ta}_3\text{S}_2$  have been reported a few decades ago, which show a semimetal behavior with MR up to about 100% at low temperatures [21]. In this work, we have successfully grown the single crystals of  $\text{Ta}_3\text{S}_2$  and performed the magnetotransport studies. We found a large positive MR =  $[\rho_{xx}(B) - \rho_{xx}(0)] / \rho_{xx}(0) \times 100\%$  up to 8000%, which is about two orders of magnitude higher than that of polycrystalline samples. The MR shows a strong anisotropic behavior when the magnetic field is rotated in the  $ab$ -plane. Hall resistivity measurement indicates that hole-type carriers with very high mobility dominate the transport properties at low temperatures, and a two-band model is sufficient to describe the large MR and its deviation from the quadratic field dependence. The analysis of the Shubnikov-de Haas (SdH) oscillations also reveals three fundamental frequencies originated from the 3D Fermi surface (FS) pockets. All these results reveal a complex electronic structure in  $\text{Ta}_3\text{S}_2$ .

## EXPERIMENT AND METHOD

The single crystals of  $\text{Ta}_3\text{S}_2$  were grown by the chemical vapor transport method [22]. Stoichiometric amounts of  $\text{TaS}_2$  and Ta powders were sealed in a Ta crucible with  $\text{TaBr}_5$  as the transport agent. The Ta crucible was then sealed in an evacuated quartz tube and the quartz tube was heated and kept at 1000 °C for 14 days before turning the furnace off. The obtained crystals were characterized by X-ray diffraction (XRD) on a PANalytical diffractometer with Cu  $K\alpha$  radiation at room temperature. MR

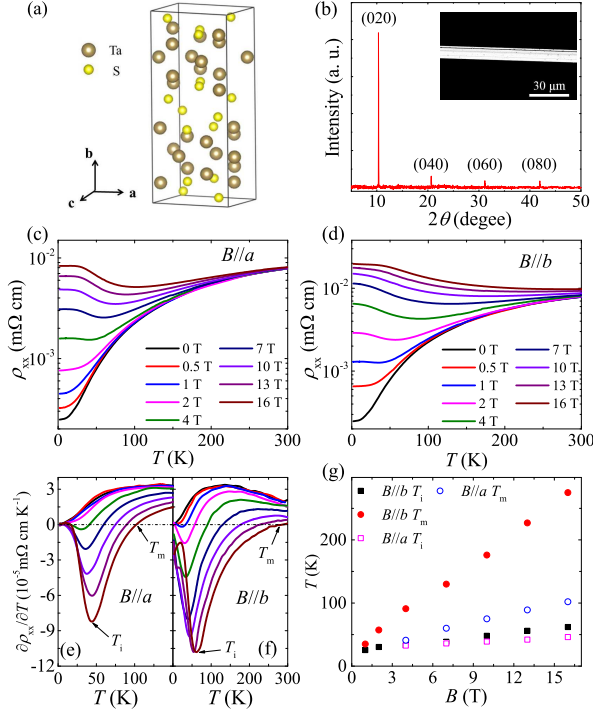


FIG. 1: (Color online)(a) The crystal structure of Ta<sub>3</sub>S<sub>2</sub> with *Abm2* space group. The brown-gray and yellow balls represent the Ta and S atoms, respectively. (b) The XRD pattern of the Ta<sub>3</sub>S<sub>2</sub> single crystal with (0*k*0) reflections. Inset: A SEM image of a ribbon-shaped sample. (c)-(d) Temperature dependence of  $\rho_{xx}$  under selected magnetic fields plotted on semi-log scale for  $B \parallel a$  and  $B \parallel b$ , respectively. (e)-(f) The derivative of resistivity  $\partial\rho_{xx}/\partial T$  for  $B \parallel a$  and  $B \parallel b$ , respectively.  $T_m$  and  $T_i$  are defined as the temperatures at which the  $\partial\rho_{xx}/\partial T$  vs.  $T$  curves change sign and take minimum, respectively. (g) Magnetic field dependence of  $T_m$  and  $T_i$ .

and Hall resistivity measurements were performed using a Quantum Design physical property measurement system (PPMS).

The obtained ribbon-shaped crystals are 10 ~ 15 mm in length, 5 ~ 10 μm in width, and 2 ~ 5 μm in thickness. Powder XRD measurement confirmed that the obtained crystals crystallize in an orthorhombic structure with *Abm2* space group. The average Ta:S atomic ratio determined by energy-dispersive X-ray (EDX) spectroscopy analysis is close to 3:2. Fig. 1(b) shows the XRD pattern of a single crystal sample. All of the peaks can be identified as the (0*k*0) reflections of Ta<sub>3</sub>S<sub>2</sub>. The inset of Fig. 1(b) shows the scanning electron microscopy (SEM) image of Ta<sub>3</sub>S<sub>2</sub> with *c*-axis being the growth direction of the ribbon.

## RESULT AND DISCUSSION

We carried out the temperature dependence of the resistivity  $\rho_{xx}$  measurements with magnetic field  $B$  parallel

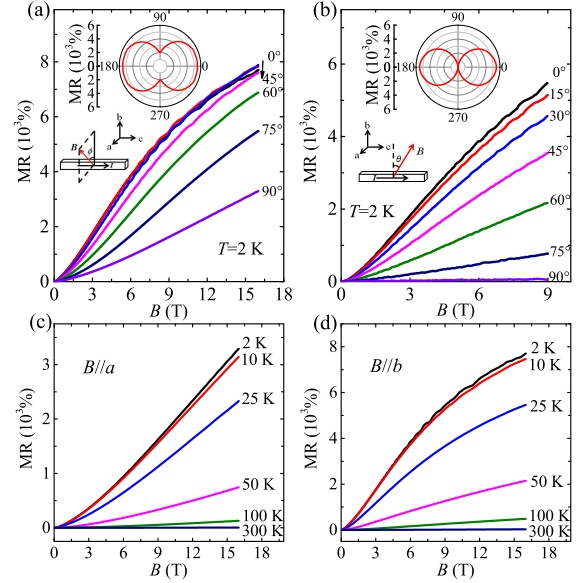


FIG. 2: (Color online)(a) Angular dependence of the MR with keeping magnetic field perpendicular to the electric current. The lower inset depicts the measurement configuration, where  $\phi$  is defined as the angle between the direction of the magnetic field and the *b*-axis of the sample. The upper inset presents polar plot of the angular dependence of the MR as the magnetic field is rotated in *ab* plane at 2 K and 9 T. (b) MR with the magnetic field applied from perpendicular ( $\theta = 0^\circ$ ) to parallel ( $\theta = 90^\circ$ ) to the electric current. The lower inset depicts the measurement configuration, where  $\theta$  is defined as the angle between the magnetic field and the *b*-axis. The upper inset shows polar plot of the angular dependence of MR, where the magnitude is taken at 2 K and 9 T. (c)-(d) Magnetic field dependence of MR at various temperatures for  $B \parallel a$  and  $B \parallel b$ , respectively.

to the crystallographic *a*-axis and to *b*-axis, as shown in Fig. 1(c) and (d), respectively. It is noted that in both configurations,  $B$  is always perpendicular to electric current  $I$ . At zero field,  $\rho_{xx}$  shows a metallic behavior with a residual resistivity ratio (RRR) up to 30, which is much higher than that of polycrystalline sample [21]. With the application of magnetic field,  $\rho_{xx}$  is enhanced drastically at low temperatures and shows a minimum, indicating that this system undergoes a field induced metal-insulator like transition. Remarkably,  $\rho_{xx}$  saturates at very low temperatures, and leads to a resistivity plateau. The magnetic field induced metal-insulator like transition and resistivity plateaus has been observed in many semimetals, including the recent discovered compounds like WTe<sub>2</sub>, TaAs, LaSb, PtSn<sub>4</sub> [8, 11, 23, 24] as well as the well-studied elements like graphite and bismuth [25, 26], but its underlying mechanism is still under debate. The resistivity plateaus have also been observed in topological insulators (TIs) such as Bi<sub>2</sub>Te<sub>2</sub>Se and SmB<sub>6</sub> in which the resistivity plateau is considered to originate from the short-circuiting effect of the metallic surface state on the

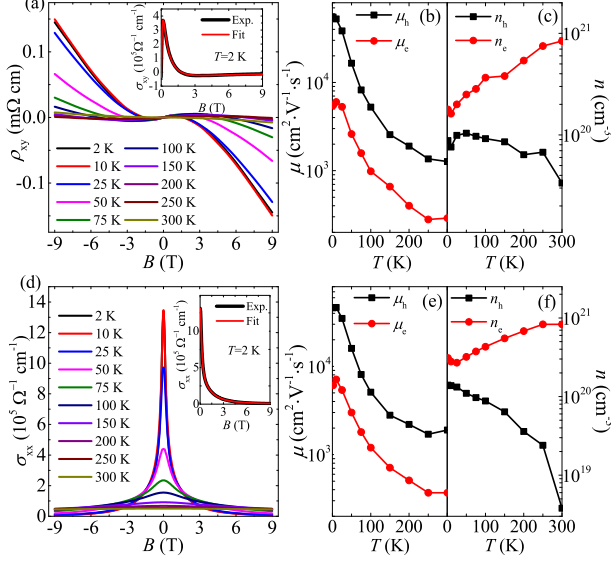


FIG. 3: (Color online) (a) The magnetic field dependence of Hall resistivity  $\rho_{xy}$  at various temperatures. The inset shows the experimental data of Hall conductivity at 2 K and the fitted curve. (b)-(c) The temperature dependence of carrier densities and carrier mobilities of electrons and holes obtained by fitting Hall conductivity  $\sigma_{xy}$ . (d) The magnetic field dependence of longitudinal conductivity  $\sigma_{xx}$ . The inset shows the experimental data of  $\sigma_{xx}$  at 2 K and the fitted curve. (e)-(f) The temperature dependence of carrier densities and carrier mobilities of electrons and holes obtained by fitting  $\sigma_{xx}$ .

bulk insulating state [27, 28]. To get a more clear view of the exotic transport behavior, we plotted the derivative  $\partial\rho_{xx}/\partial T$  curves at several magnetic fields in Fig. 1(e) and (f), respectively, where  $T_m$  and  $T_i$  are determined as the temperatures at which  $\partial\rho_{xx}/\partial T$  versus  $T$  curves change sign and take minimum, which correspond to the temperatures of the emergence of metal-insulator like transition and resistivity plateau in  $\rho_{xx}$  curves. The magnetic field dependence of the  $T_m$  and  $T_i$  is shown in Fig. 1(g). For both  $B \parallel a$  and  $B \parallel b$ ,  $T_m$  increases rapidly with increasing field, whereas  $T_i$  is almost unchanged even at high fields. The tendency of the magnetic field induced metal-insulator like transition for  $B \parallel b$  is larger than that for  $B \parallel a$ . The metal-insulator like transition was tentatively ascribed to multiband effects in the system with low carrier density and electron-hole compensation [29], or an excitonic gap induced by magnetic field [30]. However, none of the existing theories seem to account for the saturation of the low temperature resistance in a fixed magnetic field in semimetals.

The upper inset of Fig. 2(a) presents polar plot of the angular dependence of the MR measured at 2 K and 9 T as the electric current flows along the crystallographic  $c$ -axis, and the magnetic field is rotated in  $ab$ -plane. The

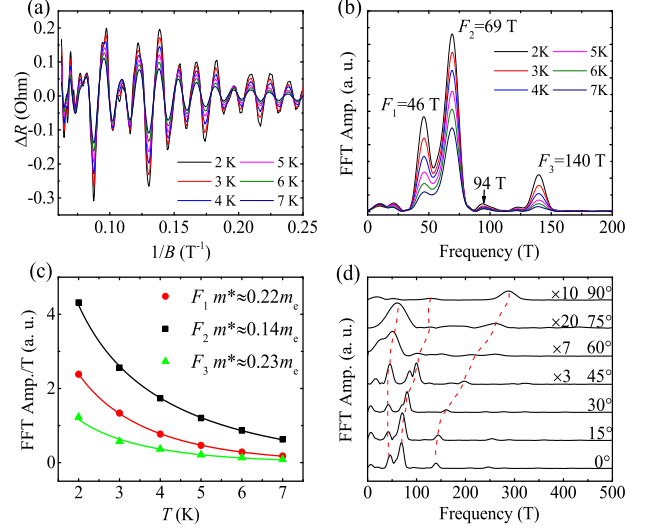


FIG. 4: (Color online) (a) SdH oscillations after subtracting background at 2-7 K for  $B \parallel b$  as a function of  $1/B$ . (b) The FFT spectra of oscillations at 2-7 K with three fundamental frequencies. (c) The oscillation amplitudes as function of temperature with fitted curves. (d) Angular dependence of the FFT spectra of the oscillations taken at 2 K by rotating the field from parallel to perpendicular to  $b$ -axis. The dashed lines are guides to the eyes.

lower inset depicts the measurement configuration, where  $\phi$  is defined as the angle between the direction of the magnetic field and the  $b$ -axis of the sample. This dipole-like pattern indicates that the MR for magnetic field along  $b$ -axis is much larger than that for magnetic field along  $a$ -axis. Fig. 2(a) shows the field dependence of MR at different  $\phi$  up to 16 T. A large MR up to 8000% is observed for  $\phi = 0^\circ$ . Near the zero field, MR presents a quadratic field dependence before a linear behavior at moderate fields, after which MR shows a tendency to saturation up to 16 T. The obvious SdH oscillations indicate the high quality of the sample. One can see that the SdH oscillations are suppressed remarkably as  $\phi$  is increased. The field dependence of the MR is also measured at 2 K by tilting the magnetic field from perpendicular to parallel to the applied current, as shown in Fig. 2(b). Dramatic drop of the MR is observed but no tendency of negative MR is detected up to 9 T for  $B \parallel I$ . The angular dependence can be more directly seen in the upper inset of Fig. 2(b), where the magnitude of the MR is taken at 9 T and 2 K.

Figure 2(c) and (d) show the magnetic field dependence of MR at various temperatures for  $B \parallel a$  and  $B \parallel b$  with keeping the magnetic field perpendicular to the electric current, respectively. In contrast to the high field saturation of low temperature MR for the magnetic field applied along  $b$ -axis ( $B \parallel b$ ), MR exhibits quadratic field dependence at low fields and becomes linear at high fields

without any trend towards saturation for the field applied along  $a$ -axis ( $B \parallel a$ ). With increasing temperature, MR drops off obviously for both two directions. Below 10 K, obvious SdH oscillations are present in the MR curves for  $B \parallel b$  above 4 T, while the SdH oscillations for  $B \parallel a$  are very weak and present only above 10 T. The difference of the amplitude of the SdH oscillations between the two directions indicates that the difference of the carrier mobility and effective mass between the two directions.

To provide some clues to understand the exotic magnetotransport properties, we performed Hall-effect measurement on the single crystal of  $\text{Ta}_3\text{S}_2$ . The magnetic field is approximately along  $b$ -axis. Figure 3(a) and (d) present the magnetic field dependence of Hall resistivity  $\rho_{xy}$  and longitudinal conductivity  $\sigma_{xx}$  at several temperatures from 2 K to 300 K. At low temperatures,  $\rho_{xy}$  has a positive slope in low field and a negative slope in high field, suggesting the coexistence of two types of carriers. At higher temperatures, the positive slope composition gradually decays and the  $\rho_{xy}$  curves tend to be linear, suggesting that electrons dominate the main transport processes. All these are consistent with multiple hole- and electron-like carriers as observed in other semimetals [6, 8, 31]. In a semiclassical two-band model, the Hall conductivity  $\sigma_{xy}$  and longitudinal conductivity  $\sigma_{xx}$  are expressed as [32, 33]:

$$\sigma_{xy} = \left[ \frac{n_h \mu_h^2}{1 + (\mu_h B)^2} - \frac{n_e \mu_e^2}{1 + (\mu_e B)^2} \right] eB, \quad (1)$$

$$\sigma_{xx} = \frac{en_e \mu_e}{1 + (\mu_e B)^2} + \frac{\sigma_{xx}(0) - en_e \mu_e}{1 + (\mu_h B)^2}, \quad (2)$$

Where  $n_e$  (or  $n_h$ ) is the carrier density of electron (or hole),  $\mu_e$  (or  $\mu_h$ ) is the mobility of electron (or hole), respectively. We find that, both of  $\sigma_{xy}$  and  $\sigma_{xx}$  can be well fitted by the two-band model. The fitting curves for  $T=2$  K are shown in the inset of Fig. 3(a) and (d), respectively. The carrier densities and mobilities obtained by fitting  $\sigma_{xy}$  and  $\sigma_{xx}$  have same order of magnitude and similar temperature dependent tendency, as shown in Fig. 3(b), (c), (e), and (f). A good agreement between the fitting of  $\sigma_{xy}$  and  $\sigma_{xx}$  indicates that two-band model is sufficient to describe the behavior of the field dependent MR. Both of the mobilities of the two type carriers decrease with increasing temperature. At  $T=2$  K, the mobility of holes,  $\mu_h \simeq 5 \times 10^4 \text{ cm}^2 \text{ V}^{-1} \text{ s}^{-1}$ , is larger than that of electrons  $\mu_e$  by one order of magnitude. Furthermore, as the temperature decreases, the electron density decreases and the hole density increases. The two carrier densities tend to be close to each other but have no possibility to compensate even at extreme low temperature. Remarkably, our results suggest that perfect electron-hole compensation is not necessary for the large MR in  $\text{Ta}_3\text{S}_2$ , and classical theory of magnetoresistance is sufficient to describe the quadratic field

dependence of MR at low fields and saturation of MR at high fields as seen in normal metals [34].

SdH oscillations are proved to be a powerful tool in the studies of topological quantum materials. Figure 4(a) shows the plots of oscillatory components  $\Delta R$  versus  $1/B$  at several temperatures, obtained by subtracting a background from the  $R(B)$  isotherms. The fast Fourier transform (FFT) analysis of these data yields three fundamental frequencies at about  $F_1 = 46 \text{ T}$ ,  $F_2 = 69 \text{ T}$ , and  $F_3 = 140 \text{ T}$ , and the weak peak at 94 T is the second harmonics of  $F_1$ , as shown in Fig. 4(b). The cyclotron masses for the three frequencies can be obtained by fitting the temperature dependent FFT amplitude using the Lifshitz-Kosevitch formula [35]:  $A \propto \frac{2\pi^2 k_B T m^* / eB\hbar}{\sinh(2\pi^2 k_B T m^* / eB\hbar)}$ , where  $k_B$  is the Boltzmann constant and  $m^*$  is cyclotron mass.  $B$  is determined by the range of oscillation:  $1/B = (1/B_1 + 1/B_2)/2$ , where  $1/B_1$  and  $1/B_2$  are the up and down limits of  $1/B$ . The fitting result is shown in Fig. 4(c). The cyclotron masses for the three frequencies are estimated to be  $0.22m_e$ ,  $0.14m_e$ , and  $0.23m_e$ , respectively. The cross-sectional area of the FS can be obtained by the Onsager relation [35]:  $F = (\Phi_0/2\pi^2)A_F$ , where  $F$  is the FFT frequency,  $A_F$  is the cross-sectional area of the FS and  $\Phi_0$  is the flux quantum. The cross-sectional areas of the three frequencies are  $4.4 \times 10^{-3} \text{ \AA}^{-2}$ ,  $6.6 \times 10^{-3} \text{ \AA}^{-2}$ , and  $1.3 \times 10^{-2} \text{ \AA}^{-2}$ , occupying 0.47%, 0.7%, and 1.4% of the cross-sectional area of the first Brillouin zone (BZ), respectively. The small ratio of the cross-sectional area of FS in the first BZ is the feature of semimetals. Fig. 4(d) shows the FFT spectra of the SdH oscillations measured at 2 K by rotating the field from parallel to perpendicular to  $b$ -axis. We note that,  $F_1$  is almost unchanged, indicating a spherical FS pocket. The other two frequencies change monotonically with rotating the magnetic field, indicating the ellipsoidal pockets.

## CONCLUSION

In conclusion, we have successfully grown the single crystals of  $\text{Ta}_3\text{S}_2$ , a robust type II WSM candidate. Large MR and anisotropic MR are observed when the magnetic field is applied perpendicular to current. The temperature dependent resistivity shows the magnetic field induced metal-insulator like transition and resistivity plateau at low temperature. The metal-insulator like transition temperature increases rapidly with increasing field, whereas the temperature of saturation of the resistivity is almost independent with magnetic field. Hall resistivity measurement reveals the high mobility of holes without the compensation of electrons and holes. The analysis of SdH oscillations reveals three FS pockets including a sphere pocket and two ellipsoidal pockets. We hope this work can provide valuable clues for further research on  $\text{Ta}_3\text{S}_2$  and other type II Weyl semimetals.

**Acknowledgements:** This work was supported by

National Basic Research Program of China 973 Program (Grant No. 2015CB921303), and the “Strategic Priority Research Program (B)” of the Chinese Academy of Sciences (Grant No. XDB07020100).

†gfchen@iphy.ac.cn

- 
- [1] X. Wan, A. M. Turner, A. Vishwanath, and S. Y. Savrasov, Phys. Rev. B **83**, 205101 (2011).
  - [2] A. A. Burkov and L. Balents, Phys. Rev. Lett. **107**, 127205 (2011).
  - [3] Z. Wang, Y. Sun, X. Q. Chen, C. Franchini, G. Xu, H. Weng, X. Dai, and Z. Fang, Phys. Rev. B **85**, 195320 (2012).
  - [4] Z. K. Liu, B. Zhou, Y. Zhang, Z. J. Wang, H. M. Weng, D. Prabhakaran, S. K. Mo, Z. X. Shen, Z. Fang, X. Dai, Z. Hussain, and Y. L. Chen, Science **343**, 864 (2014).
  - [5] Z. Wang, H. Weng, Q. Wu, X. Dai, and Z. Fang, Phys. Rev. B **88**, 125427 (2013).
  - [6] T. Liang, Q. Gibson, M. N. Ali, M. Liu, R. J. Cava, and N. P. Ong, Nat. Mater. **14**, 280 (2015).
  - [7] H. Weng, C. Fang, Z. Fang, B. A. Bernevig, and X. Dai, Phys. Rev. X **5**, 011029 (2015).
  - [8] X. Huang, L. Zhao, Y. Long, P. Wang, D. Chen, Z. Yang, H. Liang, M. Xue, H. Weng, Z. Fang, X. Dai, and G. Chen, Phys. Rev. X **5**, 031023 (2015).
  - [9] S. Y. Xu, I. Belopolski, N. Alidoust, M. Neupane, G. Bian, C. L. Zhang, R. Sankar, G. Q. Chang, Z. J. Yuan, C. C. Lee, S. M. Huang, H. Zheng, J. Ma, D. S. Sanchez, B. K. Wang, A. Bansil, F. C. Chou, P. P. Shibayev, H. Lin, S. Jia, and M. Z. Hasan, Science **349**, 613 (2015).
  - [10] B. Q. Lv, H. M. Weng, B. B. Fu, X. P. Wang, H. Miao, J. Ma, P. Richard, X. C. Huang, L. X. Zhao, G. F. Chen, Z. Fang, X. Dai, T. Qian, and H. Ding, Phys. Rev. X **5**, 031013 (2015).
  - [11] M. N. Ali, J. Xiong, S. Flynn, J. Tao, Q. D. Gibson, L. M. Schoop, T. Liang, N. Haldolaarachchige, M. Hirschberger, N. P. Ong, and R. J. Cava, Nature **514**, 205 (2014).
  - [12] K. S. Novoselov, A. K. Geim, S. V. Morozov, D. Jiang, M. I. Katsnelson, I. V. Grigorieva, S. V. Dubonos, and A. A. Firsov, Nature **438**, 197 (2005).
  - [13] Z. Fang, N. Nagaosa, K. S. Takahashi, A. Asamitsu, R. Mathieu, T. Ogasawara, H. Yamada, M. Kawasaki, Y. Tokura, and K. Terakura, Science **302**, 92 (2003).
  - [14] A. A. Soluyanov, D. Gresch, Z. Wang, Q. Wu, M. Troyer, X. Dai, and B. A. Bernevig, Nature **527**, 495 (2015).
  - [15] K. Deng, G. Wan, P. Deng, K. Zhang, S. Ding, E. Wang, M. Yan, H. Huang, H. Zhang, Z. Xu, J. Denlinger, A. Fedorov, H. Yang, W. Duan, H. Yao, Y. Wu, S. Fan, H. Zhang, X. Chen, and S. Zhou, arXiv:1603.08508.
  - [16] Y. Wu, N. H. Jo, D. Mou, L. Huang, S. L. Bud’ko, P. C. Canfield, and A. Kaminski, arXiv:1604.05176.
  - [17] F. Arnold, C. Shekhar, S. Wu, Y. Sun, R. D. d. Reis, N. Kumar, M. Naumann, M. O. Ajeesh, M. Schmidt, A. G. Grushin, J. H. Bardarson, M. Baenitz, D. Sokolov, H. Borrmann, M. Nicklas, C. Felser, E. Hassinger, and B. Yan, Nat. Comms. **7**, 11615 (2016).
  - [18] X. Yang, Y. Li, Z. Wang, Y. Zhen, and Z. Xu, arXiv:1506.02283.
  - [19] A. A. Zyuzin and R. P. Tiwari, arXiv:1601.00890.
  - [20] G. Chang, S. Y. Xu, D. S. Sanchez, S. M. Huang, C. C. Lee, T. R. Chang, G. Bian, H. Zheng, I. Belopolski, N. Alidoust, H. T. Jeng, A. Bansil, H. Lin, and M. Z. Hasan, Sci. Adv. **2**, e1600295 (2016).
  - [21] H. Nozaki, H. Wada, and S. Takekawa, J. Phys. Soc. Jpn. **60**, 3510 (1991).
  - [22] S. J. Kim, K. S. Nanjundaswamy, and T. Hughbanks, Inorg. Chem. **30**, 159 (1991).
  - [23] F. F. Tafti, Q. D. Gibson, S. K. Kushwaha, N. Haldolaarachchige, and R. J. Cava, Nat. Phys. **12**, 272 (2015).
  - [24] E. Mun, H. Ko, G. J. Miller, G. D. Samolyuk, S. L. Bud’ko, and P. C. Canfield, Phys. Rev. B **85**, 035135 (2012).
  - [25] D. E. Soule, Phys. Rev. **112**, 698 (1958).
  - [26] Z. Zhu, A. Collaudin, B. Fauqu, W. Kang, and K. Behnia, Nat. Phys. **8**, 89 (2011).
  - [27] D. J. Kim, S. Thomas, T. Grant, J. Botimer, Z. Fisk, and J. Xia, Sci. Rep. **3**, 3150 (2013).
  - [28] Z. Ren, A. A. Taskin, S. Sasaki, K. Segawa, and Y. Ando, Phys. Rev. B **82**, 241306(R) (2010).
  - [29] X. Du, S. W. Tsai, D. L. Maslov, and A. F. Hebard, Phys. Rev. Lett. **94**, 166601 (2005).
  - [30] D. V. Khveshchenko, Phys. Rev. Lett. **87**, 206401 (2001).
  - [31] C. Shekhar, A. K. Nayak, Y. Sun, M. Schmidt, M. Nicklas, I. Leermakers, U. Zeitler, Y. Skourski, J. Wosnitza, Z. Liu, Y. Chen, W. Schnelle, H. Borrmann, Y. Grin, C. Felser, and B. Yan, Nat. Phys. **11**, 645 (2015).
  - [32] N. W. Ashcraft and N. D. Mermin, *Solid State Physics* (Holt, Rinehart and Winston, New York, 1976).
  - [33] C. M. Hurd, *The Hall Effect in Metals and Alloys* (Cambridge University Press, Cambridge, 1972).
  - [34] A. A. Abrikosov, J. Phys. A: Math. Gen. **36**, 9119 (2003).
  - [35] D. Shoenberg, *Magnetic Oscillations in Metals* (Cambridge University Press, Cambridge, 1984).